Technische Universität Berlin
School IV - Electrical Engineering and Computer Science
Department of Computer Engineering and Microelectronics
Robotics and Biology Laboratory

Bachelor Thesis

Enhancing Air-Mass Control for Soft Pneumatic Actuators with Air-Flow-Sensors

presented by

Joel Simon Fuchs
Matr.-Nr.: 354546
joel.s.fuchs@campus.tu-berlin.de
Computer Science

Date of submission: **17.11.2021**
Examiners: **Prof. Dr. Oliver Brock, Prof. Dr. Jörg Raisch**
Advisors: **Prof. Dr. Oliver Brock, Adrian Sieler**

Declaration

I hereby declare in lieu of an oath that I have produced this work by myself. All used sources are listed in the bibliography and content taken directly or indirectly from other sources is marked as such.

Eidesstattliche Erklärung

Hiermit erkläre ich an Eides statt, dass ich die vorliegende Arbeit selbstständig und eigenhändig sowie ausschließlich unter Verwendung der aufgeführten Quellen und Hilfsmittel angefertigt habe.

16.11.202

Berlin, den

Unterschrift

Abstract

In this thesis we evaluate five different air flow sensors, one of which is combined with a proportional valve, for their use in mass estimation for the control of a soft robotic finger.
First, we test their behaviour regarding different unidirectional actuated trajectories. The results show that for most of the sensors further calibration is necessary to obtain usable data. We present a simple calibration method to improve the results.
Afterwards, we chose two sensors to implement and test a bidirectional mass estimator.
We argue that while the results are comparable to the existing mass estimator, further research into the effects of flow profiles on the sensors is necessary.
Furthermore, we conclude that the use of proportional valves significantly improves the motion of the finger regarding shivers in contrast to the currently used binary valves.

Zusammenfassung

Titel:
Verbesserung der Luftmassenregelung weicher pneumatische Aktuatoren mit Luftfluss-Sensoren

In dieser Arbeit evaluieren wir fünf verschiedene Luftfluss-Sensoren für ihren Einsatz in der Massenabschätzung zur Steuerung eines weichen Roboterfingers. Einer der Sensoren ist Teil einer Kombination aus einem proportionalen Ventil und einem Massenfluss-Sensor.
Zuerst testen wir ihr Verhalten bezüglich unterschiedlicher unidirektionaler Trajektorien. Die Ergebnisse zeigen, dass für die meisten Sensoren eine weitere Kalibrierung erforderlich ist, um verwertbare Daten zu erhalten. Um die Ergebnisse zu verbessern, stellen wir eine einfache Kalibrierungsmethode vor.
Wir wählen zwei Sensoren aus, um einen bidirektionalen Massenabschätzer zu implementieren und zu testen.
Die Ergebnisse zeigen, dass dieser zwar mit dem bestehenden Massenschätzer vergleichbar ist, jedoch weitere Untersuchungen zu den Auswirkungen von Strömungsprofilen auf die Sensoren erforderlich sind.
Darüber hinaus kommen wir zu dem Schluss, dass der Einsatz von Proportionalventilen das Zittern in der Bewegung der Finger im Vergleich zu den momentan verwendeten Binärventilen deutlich verbessert.

Contents

List of Figures

List of Tables

1 Introduction

Actuating a soft pneumatic robot hand is not as straightforward as actuating a rigid robot hand. While rigid hands mostly have a small number of Degrees of Freedom that are precisely controllable using joint encoders, this is not the case for soft pneumatic hands [1]. Soft pneumatic hands have a nearly infinite number of Degrees of Freedom and it is therefore not possible to control the exact state of the hand at any given moment. They also make use of mechanical compliance or morphological computation to alter their shape when in contact with the environment to improve the desired actuation without the need for additional control software or sensors [2] [3]. Therefore, the behavior of a soft pneumatic actuator is influenced by the compliant shape adaptation of the hand that is governed by the physical properties of the body as well as the control input. Only the latter can be influenced via pneumatic control and is therefore the focus of this thesis.
Even though pressure is often used as a control variable for soft pneumatic actuators, air mass is preferable as it is independent of the volume change occurring while e.g. grasping an object and was therefore chosen for the RBO Hand 2 [4].
This is done with a data-driven mass controller using binary valves and pressure sensors as mass-flow sensors or proportional valves were not available in the desired flow range at that time [5]. While it demonstrates the advantages of mass control it also has its limitations, especially drift over time. In recent years, suitable sensors and valves have become commercially available and might be a solution to this problem. Since air mass is not directly measurable in a practical way for this application the first derivative or air flow is chosen instead and integrated over time.
We start by giving an overview over existing control methods for soft pneumatic actuators and mass control. Then we will establish requirements for the mass-flow sensors based on experience working with the RBO Hand 2 of the Robotics and Biology Lab (RBO) at TU Berlin. Next we will introduce the sensor technology used in these sensors and present the characteristics of each individual sensor. In the main part we will explain the experiments and discuss the results for each sensor.
Based on that we will choose sensors to implement a mass estimator based flow integration and show the results compared to the existing controller.
We will show that proportional valves offer an improvement regarding the smoothness of motion. While none of the tested air-flow sensors fit our use-case perfectly, we show that a comparable performance to the existing estimator can be accomplished and potentially improved upon with a more fitting sensor.

2 Related Work

There are several approaches to control a pneumatic actuated soft robot [6].
An open-loop or time-based control method is based on predetermined timed openings of the control valves to actuate the desired position of the manipulator. This is a quick and cost effective way since it does not need sensors or a more complex control algorithm. It is also more error prone compared to other approaches as it lacks a way to counteract influences induced by changes to the electric, pneumatic or physical system, e.g. a volume change when manipulating an object with a soft robotic hand.
A common closed-loop control mechanism uses the pressure in the pneumatic system as the control variable [7]. This is a simple and robust technique as pressure is directly measurable and a control input directly entails a pressure change that can be assumed to be instant throughout the system.
The position-based control method tries to control the position of a soft pneumatic actuator by modeling the behaviour e.g. through the piecewise constant curvature model (PCC), learned model using neural networks or making use of an external camera for visual servoing [8][9][10].
In contrast to these approaches, the equilibrium-point control is focused on enabling compliant motions from a soft robot to improve behaviour without further direct control inputs [6]. This is done by actuating the equilibrium point or the position the soft actuator would assume without external influences rather than trying to force it into a concrete position. Therefore, mass is chosen as a control variable instead of e.g. pressure as the mass inside a pneumatic system does not change when a volume change occurs while making contact. As compliance is an important part of soft robotics this method is used for the control of the RBO Hand 2.

3 Background

3.1 Existing Mass Estimator for the RBO Hand 2

The existing mass is based on a data-driven model developed by R. Deimel in the RBO Lab that computes the air mass change by measuring the difference between the supply pressure and the pressure in the pneumatic system [5]. The mass change is then integrated over time to obtain the air mass.
The precise structure of the soft actuator is normally not known and different fluid dynamic properties can cause an increasing error over time. Therefore, the estimator uses parameters to reduce the influence of sensor bias, friction inside the flow path, behavior of chokes to reduce the air flow and influences by dead volumes and valve timings.
These parameters are obtained via linear regression using a setup with a fixed volume and known ranges of pressures and valve opening durations. For a normal calibration 200 data points per channel or flow path are necessary. This can be done automatically.
Deimel also identifies drift, potential leakage and hysteresis as limitations for this method and suggests additional sensors or different valves to improve the behaviour.

3.2 Background MEMS Air Flow Sensors

Micro electromechanical systems or MEMS Air flow sensors can be classified into two categories: non-thermal and thermal flow sensors [11].
Non-thermal flow sensors use a mechanical working principle to measure air flow. This can be achieved by either monitoring the effect of the drag force on a cantilever in the air flow, measuring the pressure difference caused by a flow in a known channel or using a coriolis mass flow resonator [12][13]. All these methods are density dependent and therefore need temperature compensation which is not ideal.
Thermal flow sensors use the influence of the air flow on a heater element to determine the current air flow. They measure air mass flow instead of volume flow and are consequently temperature independent. Hot-wire sensors function either by identifying the difference in temperature for a heating element inside the flow with a constant heating power or the difference in power necessary to keep it at a constant temperature. Thermal mass flow sensors or calorimetric sensors use the asymmetric temperature distribution around a heating element normally on the wall

of the flow chamber. Time-of-flight sensors are a different kind of thermal mass sensor that measures the time that a pulse from the heating element needs to reach a temperature sensor [11][14].

4 Requirements

The goal is to improve on the existing data driven mass estimator while maintaining its features.
As briefly mentioned in section 3.1, three limitations have been identified: drift, leakage and hysteresis.
Experience has shown that leakage occurs rarely in practice and therefore, is negligible. Deimel proposed the use of additional sensors to combat drift and the adoption of different valves to reduce the impact of hysteresis [5].

In a perfect world we would have a constant continuous stream of accurate data from the sensor which we could add up instantly. Since this is not possible, we have to assume each value as the average value since the last read from the sensor.
This is sufficient if:

- The sensor's reaction time or the time between a change of flow and the change of the sensor value is fast enough.
- The time step between readings is small enough so that the change in flow can be regarded as linear.
- The sensor is able to detect the air flow with an adequate precision over the whole range of possible air flows.

The second point depends on the external ADC used to capture the signal for analog sensors or on the digital interface if one is provided by the manufacturer. In both cases the speed can be assumed to be fast enough for our use case and does not have to be tested individually.
Additionally, the sensors need to be able to handle pressure values up to 300 kPa.

Therefore, we need to evaluate the sensors regarding reaction time, precision, air flow and pressure range.

5 Sensors

In the following section we give a short introduction into the general function of the tested air flow sensors.
After that we present an overview of the key data for each sensor.

5.1 MEMS Thermal Mass Flow Sensors

All of the tested sensors are thermal mass flow sensors. These sensors measure the heat distribution around a heating element which is placed at the edge of the airflow.

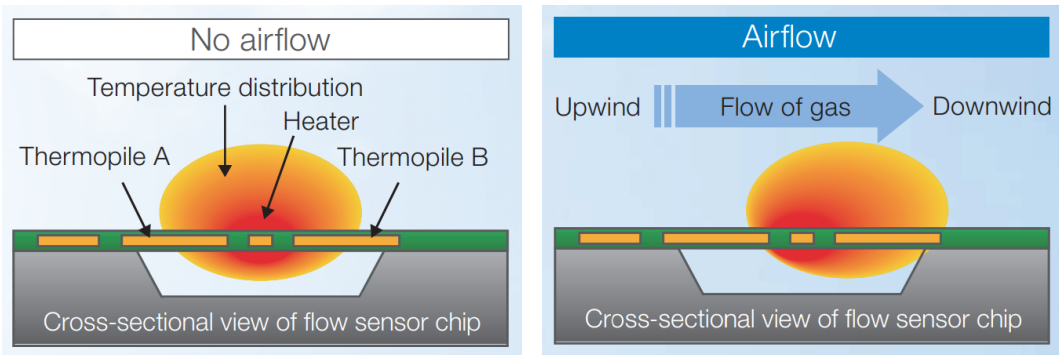

(a) Heat distribution without airflow **(b)** Heat distribution with airflow

Figure 5.1: Functionality of a thermal mass flow sensor [15]

5.2 Unit Conversion

While the measured value is air mass flow it is common for air flow sensors to express it as volume flow at a reference condition.
Therefore, we need to convert the volumetric flow in Standard Liter per Minute (SPLM) to mass flow in milligram of air per second [16].
This is done using the ideal gas law:

$$P \cdot V = m \cdot R_s \cdot T$$
$$P \cdot Q = \dot{m} \cdot R_s \cdot T$$

with:
P: Pressure
V: Volume
m: Mass
$\dot{m}$: Mass flow
n: Number of moles of gas
R: Universal gas constant
R_s: Specific gas constant
T: Temperature
Q: Volumetric flow

Example: To convert the 1 L/min measured by the Omron D6F-P0010A1 we have to adjust the formula:

$$\dot{m} = \frac{P}{R_s \cdot T} \cdot Q$$

Then we have to insert the reference conditions of the sensor and the specific gas constant of air. In this case $T = 0°\text{C}$, $P = 101.3$ kPa and $287.058 \frac{J}{kg \cdot K}$:

$$\dot{m} = \frac{101.3 \cdot 1000^2}{287.058 \cdot 273.15K \cdot 60} \cdot 1 \frac{mg}{s}$$

This gives us the conversion factor for this specific sensor:

$$\dot{m} = 21.537 \frac{mg}{s}$$

5.3 Tested Sensors

5.3.1 Festo VEMD

Figure 5.2: Festo VEMD [17]

The Festo VEMD is a proportional piezo 2-way valve with an integrated unidirectional flow controller [17]. It is actuated by setting the desired flow via an analog signal between 0-10 V. The current flow can also be obtained using an analog connection in the corresponding range.
The theoretical maximum flow possible is 20 L/min at 0°C and 101.3 kPa or about 430 mg/s. To reduce the complexity of the experiment setup we only actuated up to half of the possible maximum which proved to be sufficient.
While the valve can withstand up to 600 kPa, it is only rated up to an operating pressure of 250 kPa. This does not fulfill the requirement regarding pressure but is negligible since it does not restrict the flow range.

5.3.2 Honeywell AWM 5101 VN

Figure 5.3: Honeywell AWM 5101 VN [18]

The Honeywell AWM 5101 VN is an unidirectional analog air flow sensor with a flow range of up to 5 L/min at 0°C and 101.3 kPa which translates to about 107 mg/s [18]. This is lower than the desired flow range.
The maximum pressure for this sensor is 344 kPa.

5.3.3 Omron D6F-P0010A1

Figure 5.4: Omron D6F-P0010A1 [15]

The Omron D6F-P0010A1 is also an unidirectional analog air flow sensor [15].
With a flow range of only 1 L/min at 0°C and 101.3 kPa or 21.5 mg/s this sensor is part of the experiments to evaluate the influence of a smaller flow range regarding precision.
The maximum pressure of 50 kPa also disqualifies this particular sensor for an actual use in our case.

5.3.4 The Posifa 83020-B

Figure 5.5: Posifa 83020-B [19]

The Posifa 83020-B is a bidirectional air flow sensor with the possibility to use either a digital I2C or an analog connection to read the sensor values [19].
The flow range is with 20 L/min at 0°C and 101.3 kPa or 430 mg/s similar to the Festo VEMD and therefore meets the requirements.
With 344 kPa the maximum pressure is also sufficient.

5.3.5 Sensirion SFM 3400 AW

Figure 5.6: Sensirion SFM 3400 AW [20]

The Sensirion SFM 3400 AW is a bidirectional digital air flow sensor [20]. Like the Posifa 83020-B I2C it is used to connect to the sensor.
It has the highest flow range of the tested sensors with 33 L/min at 0°C and 101.3 kPa or 710 mg/s.
The maximum allowed pressure is with 110 kPa only a third of the required pressure range.
The Sensirion is the only temperature compensating sensor. As we are not interested in the volume flow but in the mass flow, we have to revert this by applying a factor $t = \frac{T_x}{T_s}$ where T_x is the temperature at time of measurement and T_s is the temperature at reference condition or in this case 0°C.

6 Experiments Unidirectional Mass Estimator

6.1 Setup

The experiment setup consists of two Festo proportional flow control valves for inflation and deflation. To estimate the air mass in the system, the readings from the air flow sensors are integrated over time. Additionally, the setup contains a MPX4250D pressure sensor to compute the ground truth mass using the Ideal Gas Law shown in 5.2 and the known total volume of our system. The test tube is an interchangeable volume of predetermined size. A LabJack u6 was used to control the valves and capture all data from both analog and digital sensors.
Four different trajectories were actuated with an open loop control to test the sensors.

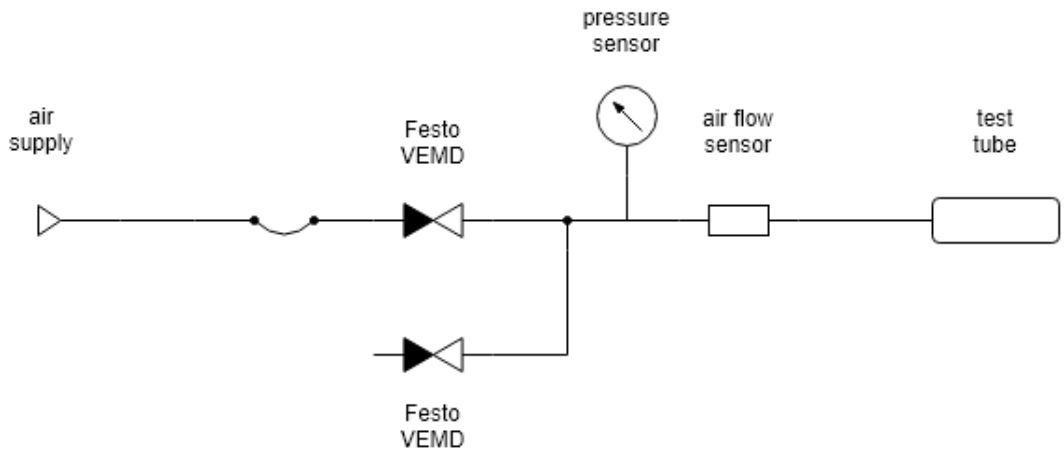

Figure 6.1: Schematic diagram of the pneumatic setup

6.2 Time Delay

To determine the basic reaction time or the delay between a flow change occurring and the measurement of each sensor, we actuate a constant flow. The shift along the x-axis between ground truth and estimated mass equals the delay in time.

6.2.1 Festo VEMD

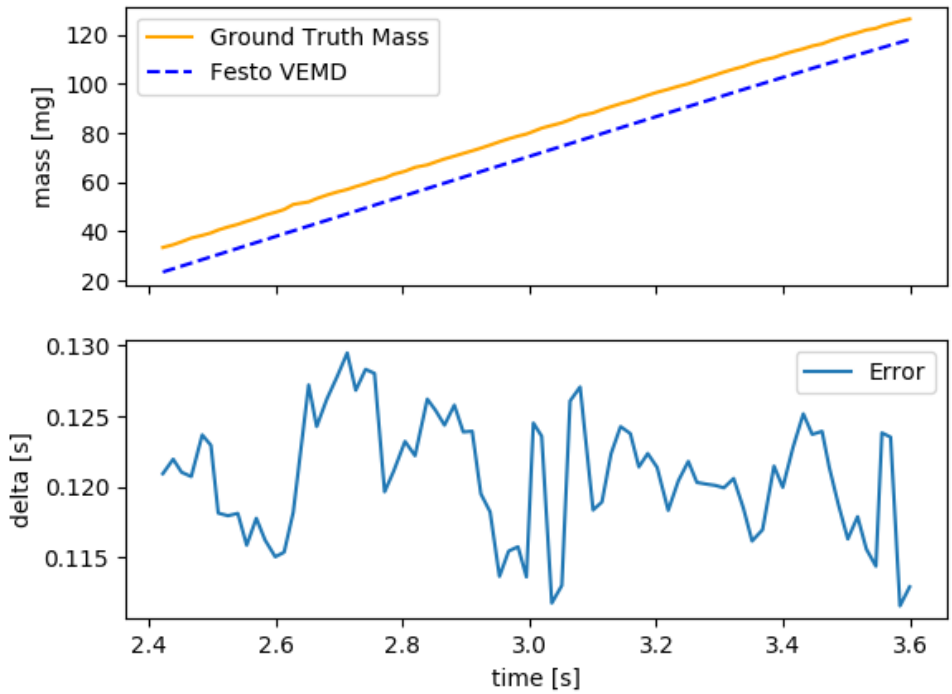

Figure 6.2: Time Delay - Festo VEMD

6.2.2 Honeywell AWM 5101 VN

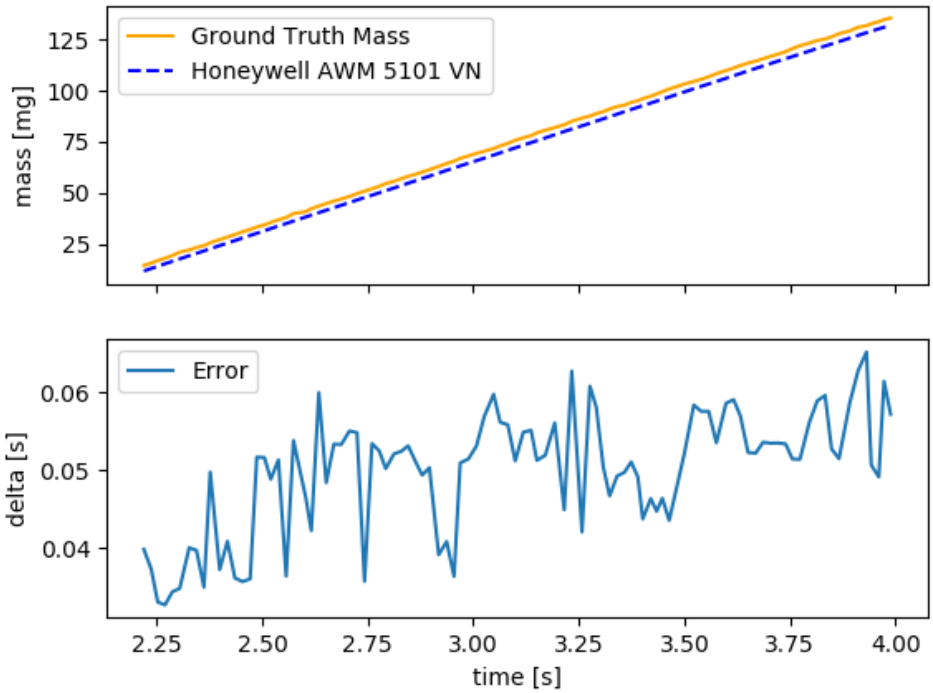

Figure 6.3: Time Delay - Honeywell AWM 5101 VN

6.2.3 Omron D6F-P0010A1

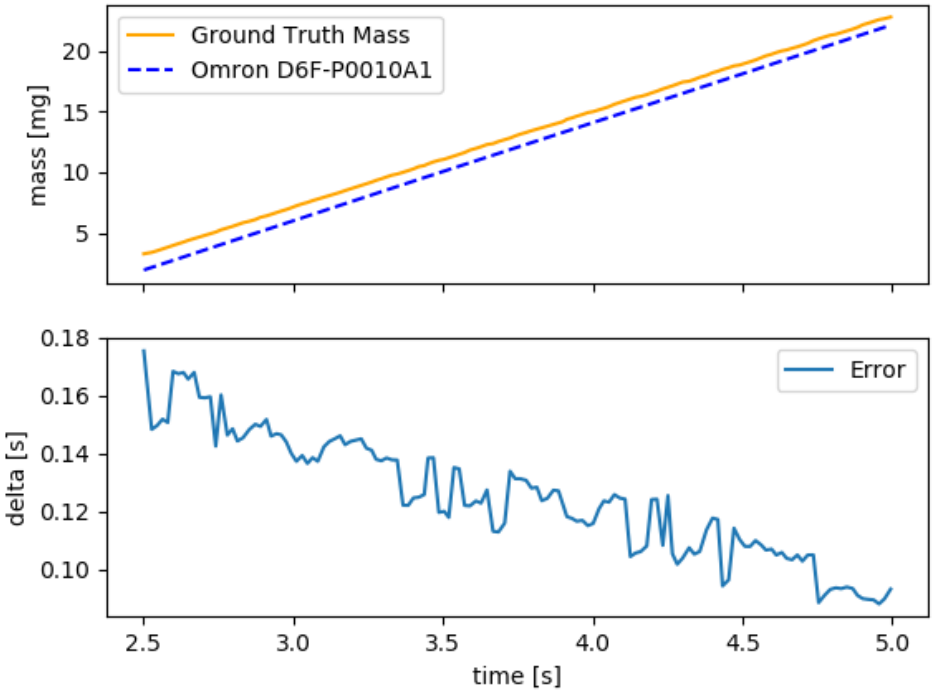

Figure 6.4: Time Delay - Omron D6F-P0010A1

6.2.4 Posifa 83020-B

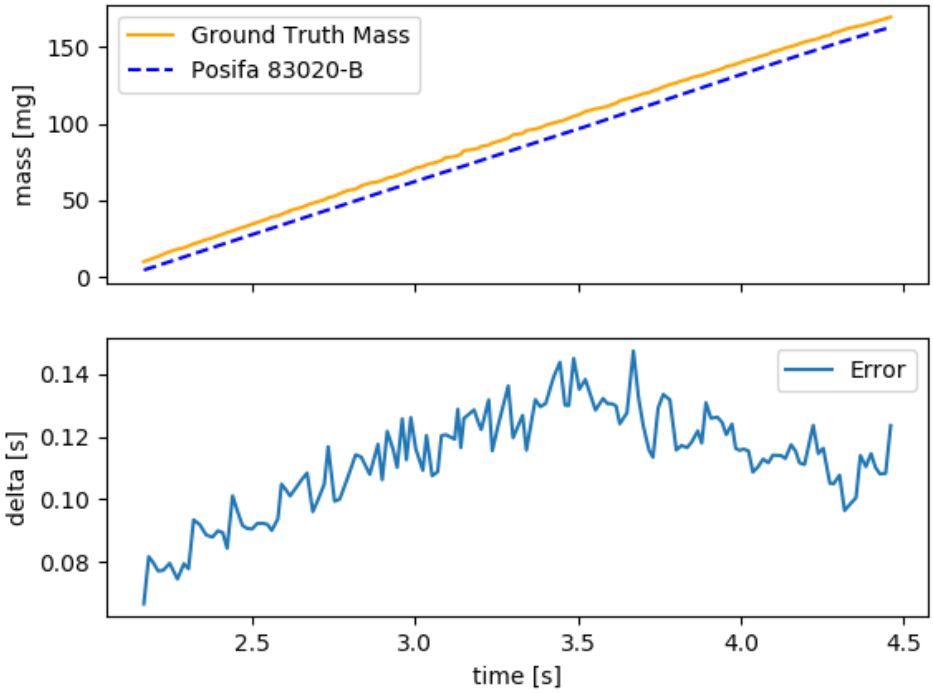

Figure 6.5: Time Delay - Posifa 83020-B

6.2.5 Sensirion SFM 3400 AW

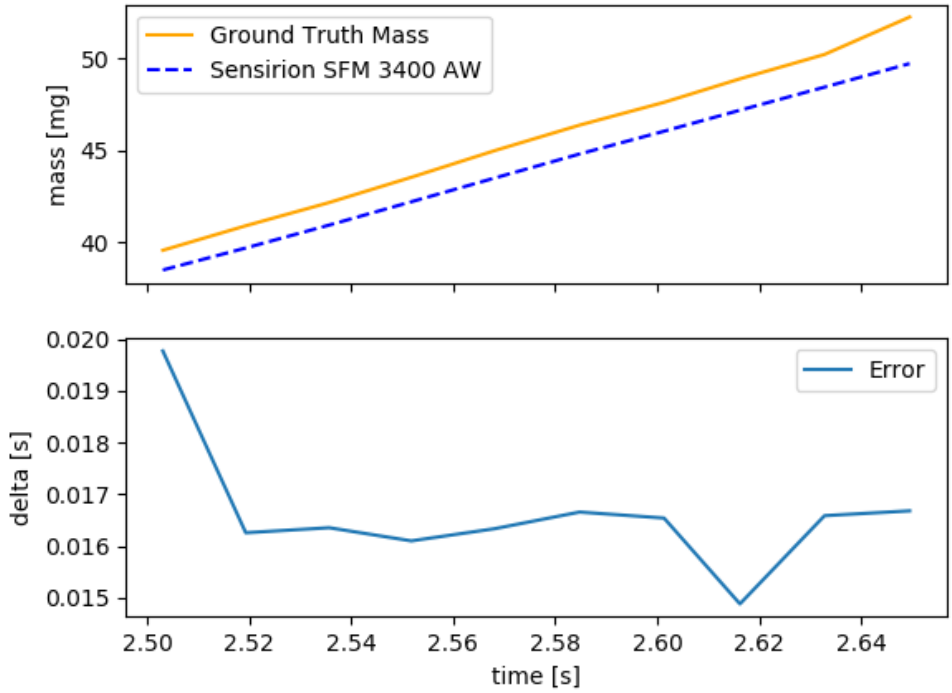

Figure 6.6: Time Delay - Sensirion SFM 3400 AW

6.2.6 Discussion

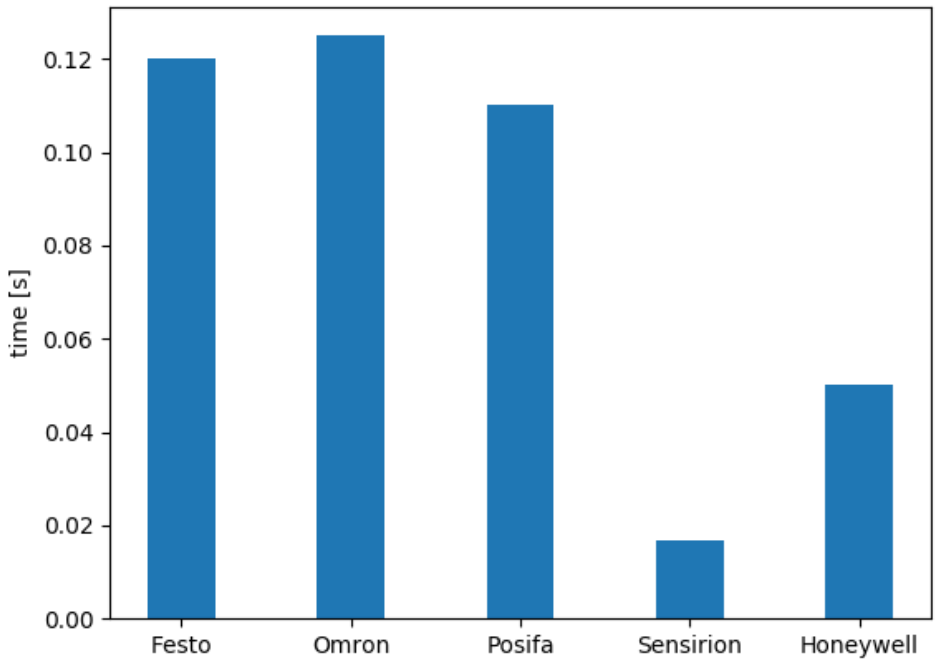

Figure 6.7: Comparison of the time delay of all tested sensors

As shown in 6.7, the Festo, Omron and Posifa sensors all have a similar delay between the ground truth mass reaching a certain value and the estimator based on the respective sensor reaching the same value of about 0.12 seconds. This is not a problem with our current setup as the Festo sensor is our limiting factor for actuation. However, for use with different valves or applications that require a faster actuation, the sensors by Honeywell or Sensiron are more suitable as their reaction times are significantly shorter.

6.3 Out of the Box

To test the sensors, we actuated four different trajectories with an open loop control. One was a linear trajectory, one a modified sinus trajectory, one a random trajectory and one a step trajectory mimicking the behavior of binary valves. As not all sensors are bidirectional, we modified the sinus and random trajectory to be monotonically non-decreasing.

6.3.1 Festo VEMD

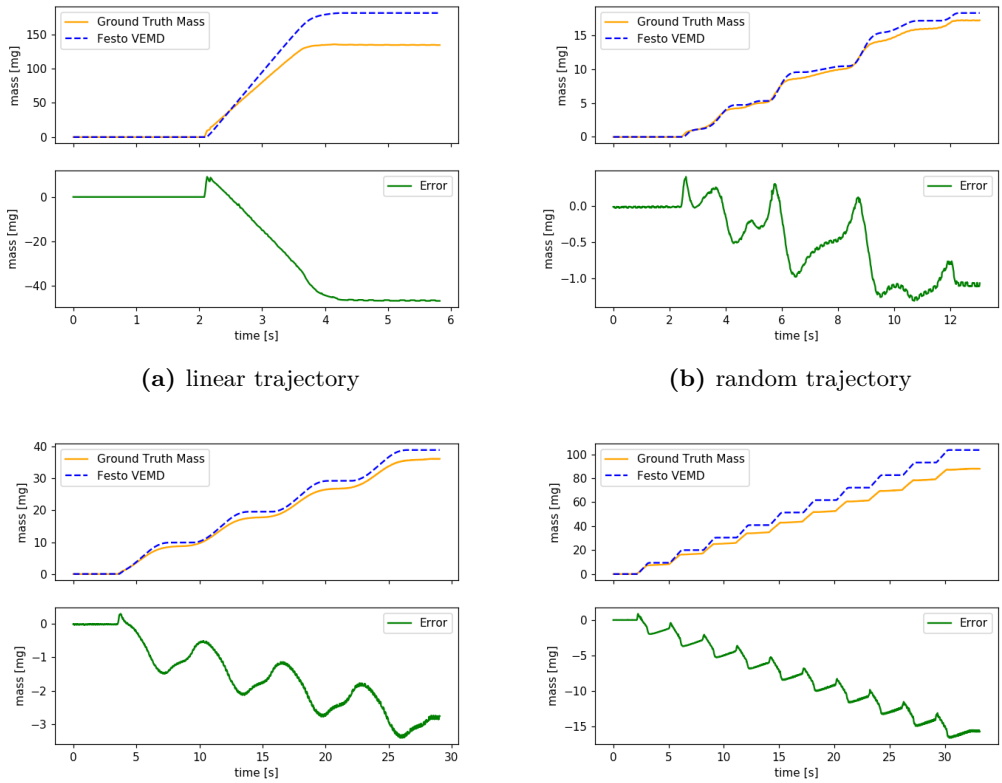

(a) linear trajectory

(b) random trajectory

(c) sinus trajectory

(d) step trajectory

Figure 6.8: Festo VEMD without calibration

6.3.2 Honeywell AWM 5101 VN

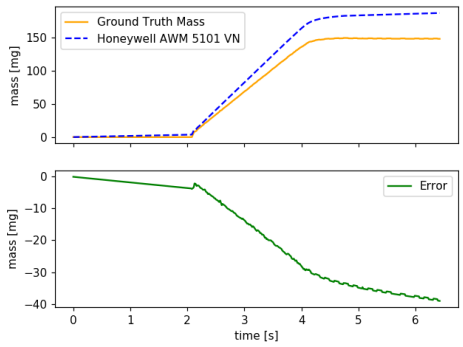

(a) linear trajectory

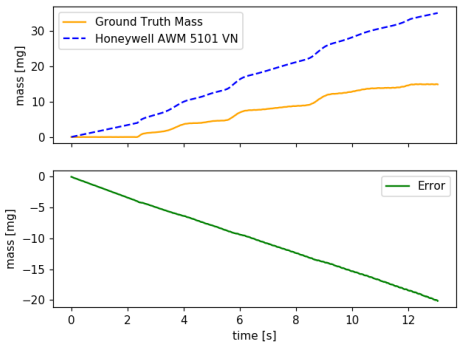

(b) random trajectory

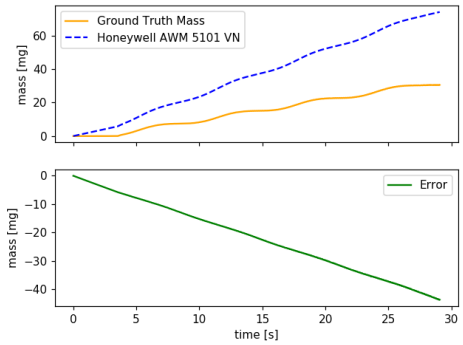

(c) sinus trajectory

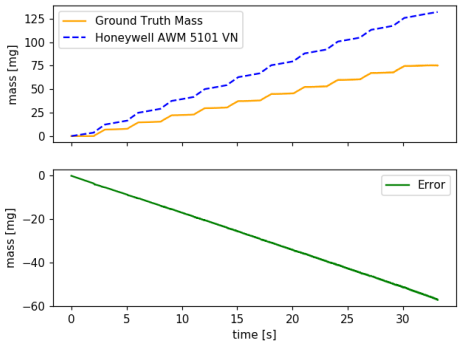

(d) step trajectory

Figure 6.9: Honeywell AWM 5101 VN without calibration

6.3.3 Omron D6F-P0010A1

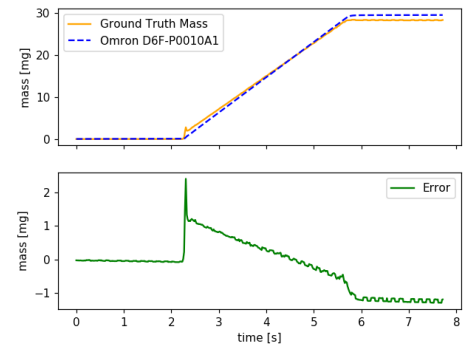

(a) linear trajectory

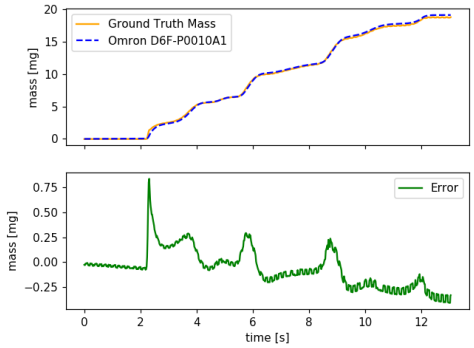

(b) random trajectory

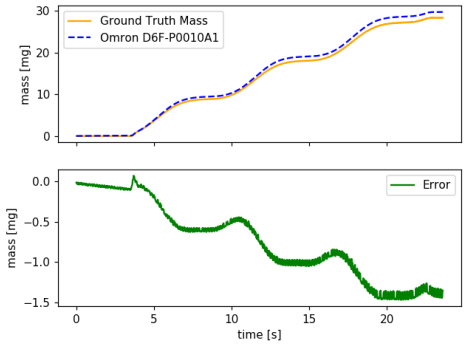

(c) sinus trajectory

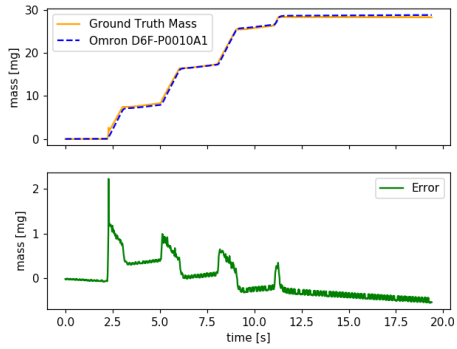

(d) step trajectory

Figure 6.10: Omron D6F-P0010A1 without calibration

6.3.4 Posifa 83020-B

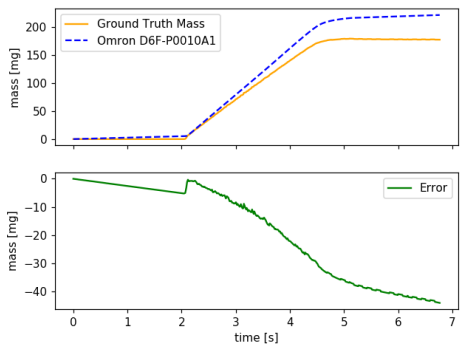

(a) linear trajectory

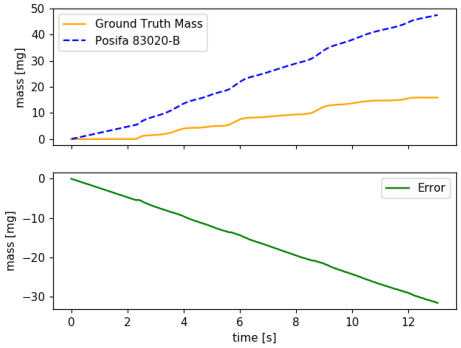

(b) random trajectory

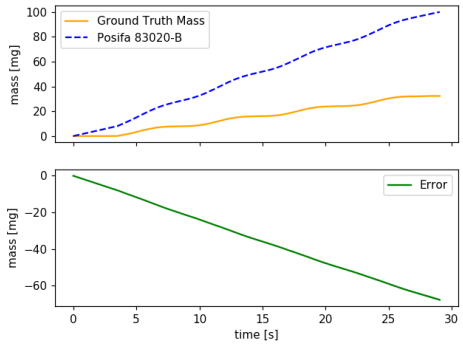

(c) sinus trajectory

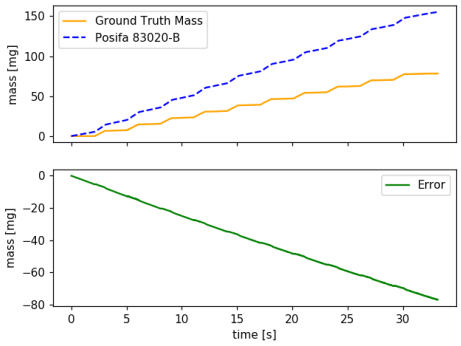

(d) step trajectory

Figure 6.11: Posifa 83020-B without calibration

6.3.5 Sensirion SFM 3400 AW

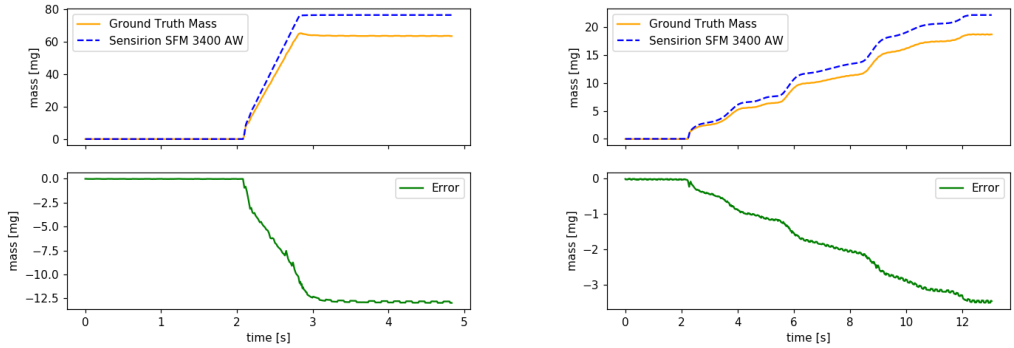

(a) linear trajectory

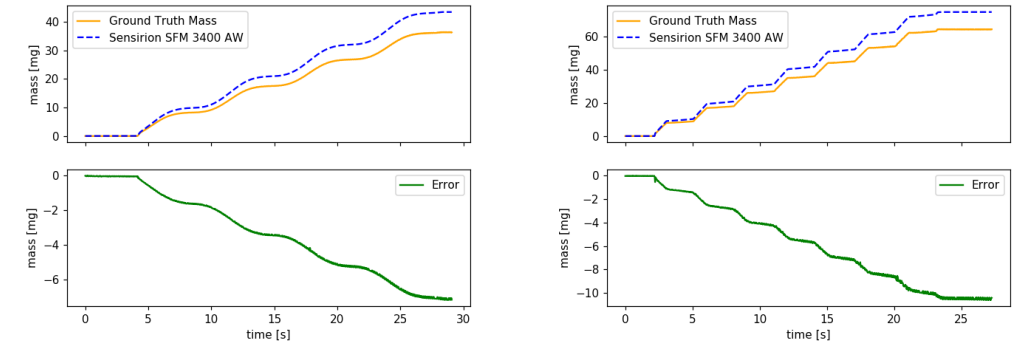

(b) random trajectory

(c) sinus trajectory

(d) step trajectory

Figure 6.12: Sensirion SFM 3400 AW without calibration

6.3.6 Discussion

With the exception of the Omron D6F-P0010A1, all sensors have an error that makes them unusable out of the box without further calibration.
However, there is a pattern that the error for all sensors is bigger when the linear trajectory is actuated. As this trajectory results in higher mass flows compared to the other trajectories, we can assume that all sensors are more precise for lower air flows.
Also, a smaller flow range does not indicate higher precision. While the Omron D6F-P0010A1 has both the smallest range and the best precision, the Sensirion SFM 3400 AW with a flow range of 710 mg/s shows better results than the Honeywell AWM 5101 VN with 107 mg/s.
A source for the error might lie in the physical shape of the different sensors. All, except the Omron D6F-P0010A1, have a tubular design. The standard pneumatic tubes used in the setup have a diameter of 0.2 cm. In comparison ,the diameter of the pneumatic connectors for the Honeywell AWM 5101 VN, Posifa 83020-B and Sensirion SFM 3400 AW are bigger. This can lead to an effect called "Jetting Condition" as seen in 6.13 which occurs as the air flow leaves the smaller tube and not immediately evenly disperses itself in the bigger tube [21]. This can lead to the sensors underestimating the actual air flow. Figure 6.14 shows the difference in the perceived mass if the test tube is removed in contrast to the closed test setup using the Posifa 83020-B as an example.
The Omron D6F-P0010A1 has a special flow path meant to separate dust particles from the air flow. Therefore, we can assume that errors induced by disadvantageous flow profiles do not affect the sensor as much. This could be an explanation for significantly better results.

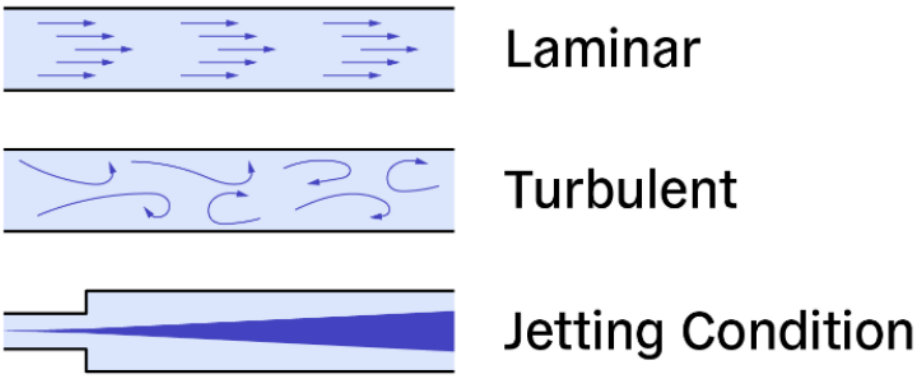

Figure 6.13: Different flow profiles passing through a tubing set [21]

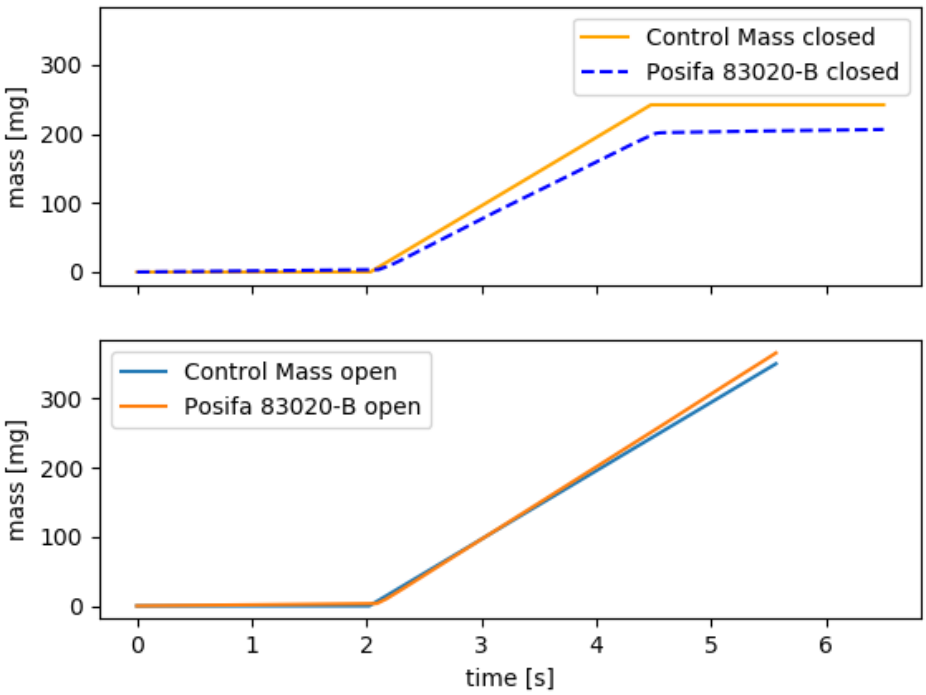

Figure 6.14: Comparison open and closed pneumatic circuit

6.4 Calibration

For all sensors the error has also a linear characteristic and which is why we propose a simple calibration method similar to the two-point calibration to improve the results [12]:

1. An offset that is computed by measuring and averaging the output of the sensor for a zero air flow.
2. A factor that is the ground truth divided by the actual sensor reading. The values are ideally taken near the high end of the sensor range. For this test we used the linear trajectory to determine this factor.

The calibrated mass flow is computed using the following formula:

$$\dot{m}_{calibrated} = (\dot{m}_{raw} - offset) \cdot factor$$

An overview of the calibration factors for each sensor can be found in Table 6.1.

Sensor	Factor	Offset
Festo VEMD	0.737	0.016
Honeywell AWM 5101 VN	0.844	-0.069
Omron D6F-P0010A1	0.976	0.008
Posifa 83020-B	0.870	0.072
Sensirion SFM 3400 AW	0.832	0.000

Table 6.1: Overview Calibration Values

6.5 Evaluation Calibration

6.5.1 Festo VEMD

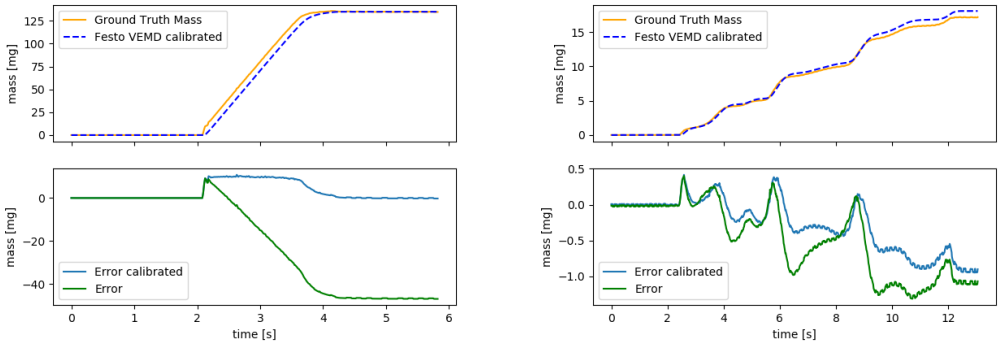

(a) linear trajectory

(b) random trajectory

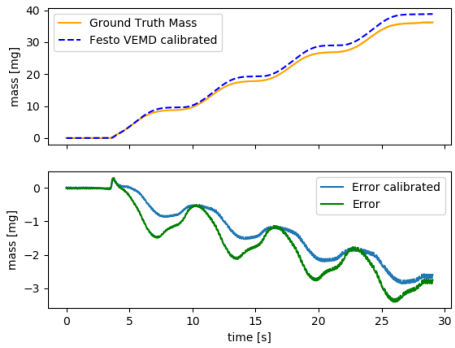

(c) sinus trajectory

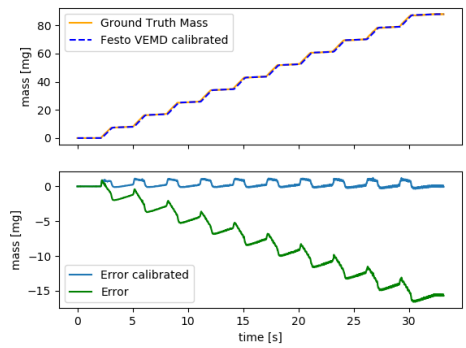

(d) step trajectory

Figure 6.15: Festo VEMD with calibration

6.5.2 Honeywell AWM 5101 VN

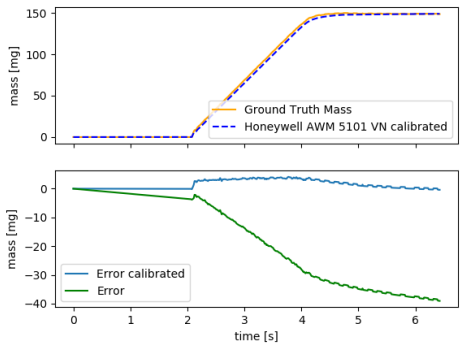

(a) linear trajectory

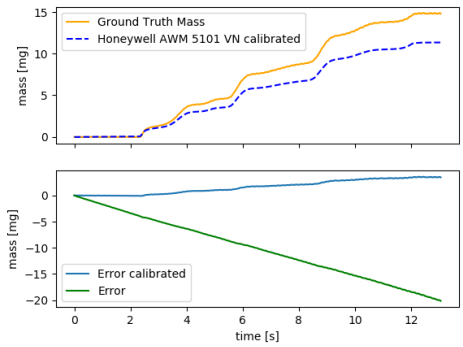

(b) random trajectory

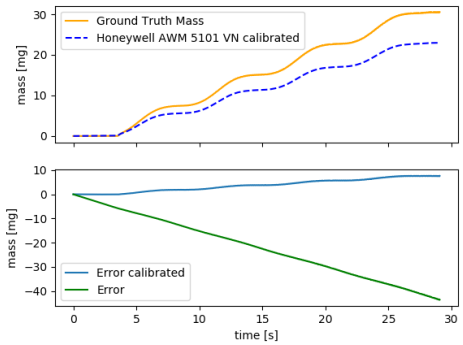

(c) sinus trajectory

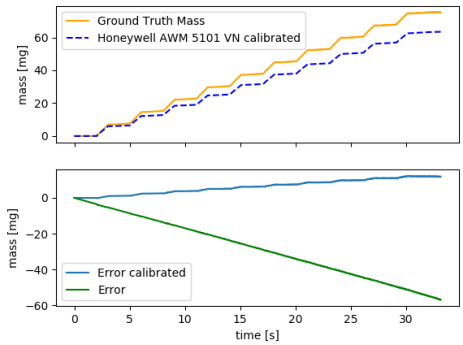

(d) step trajectory

Figure 6.16: Honeywell AWM 5101 VN with calibration

6.5.3 Omron D6F-P0010A1

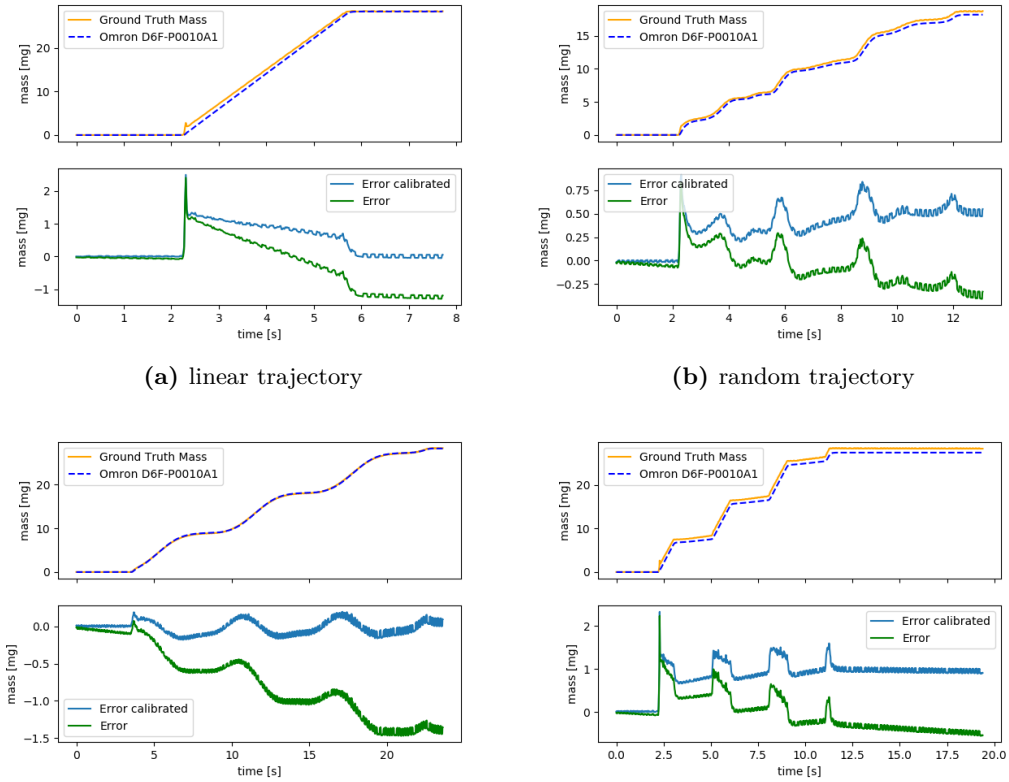

(a) linear trajectory

(b) random trajectory

(c) sinus trajectory

(d) step trajectory

Figure 6.17: Omron D6F-P0010A1 with calibration

6.5.4 Posifa 83020-B

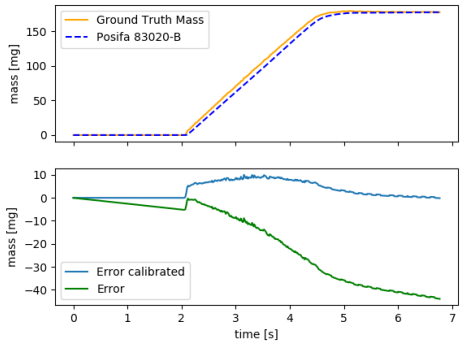

(a) linear trajectory

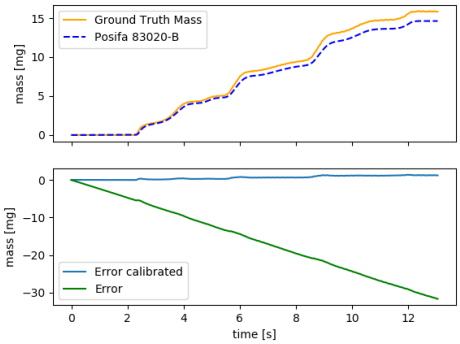

(b) random trajectory

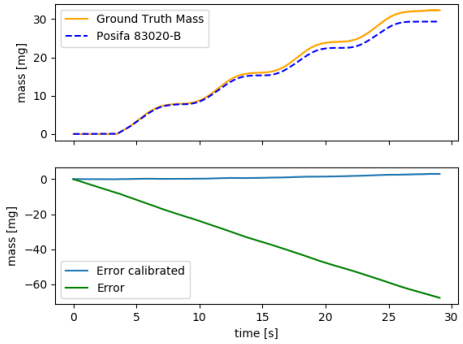

(c) sinus trajectory

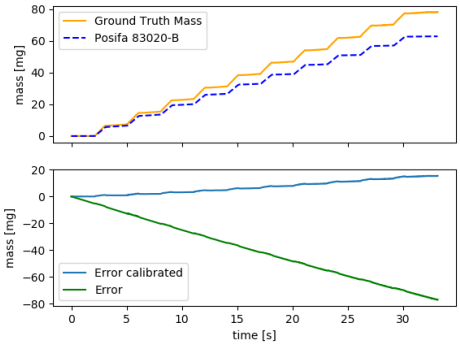

(d) step trajectory

Figure 6.18: Posifa 83020-B with calibration

6.5.5 Sensirion SFM 3400 AW

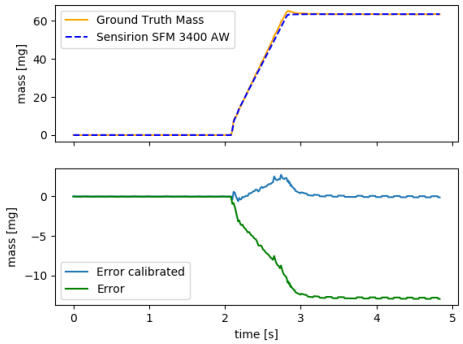

(a) linear trajectory

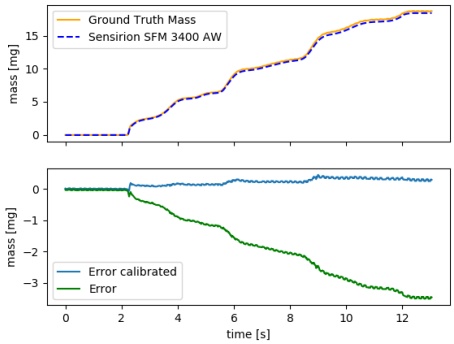

(b) random trajectory

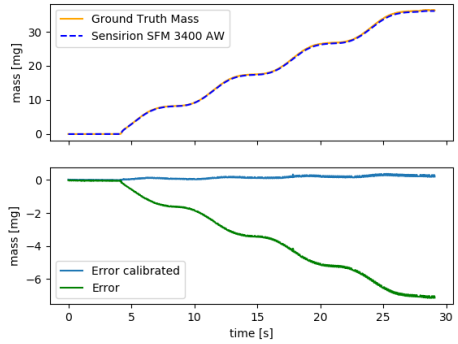

(c) sinus trajectory

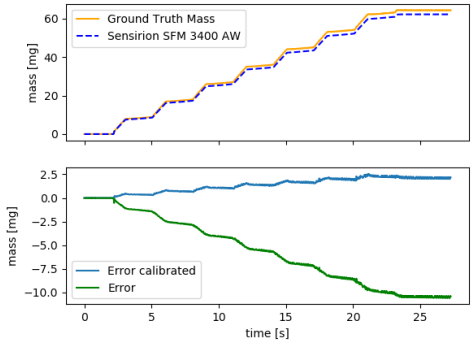

(d) step trajectory

Figure 6.19: Sensirion SFM 3400 AW with calibration

6.5.6 Discussion

We are able to achieve a notable improvement in precision with the calibration. While the factor computed using linear trajectories delivers good results, for the other trajectories there seems to be a bias towards higher mass flows. Therefore, a factor tuned to the specific flow range used in an application improves the results for this range.
Especially the results for Honeywell AWM 5101 VN and Posifa 83020-B look promising albeit the precision still lacks behind the other sensors.
An exception is the Omron D6F-P0010A1 where only two out of four trajectories show a smaller error. This is in part caused by a spike in the actuation at the beginning of the trajectory.
The calibration is also fairly robust to volume change as can be seen in Figure 6.20.

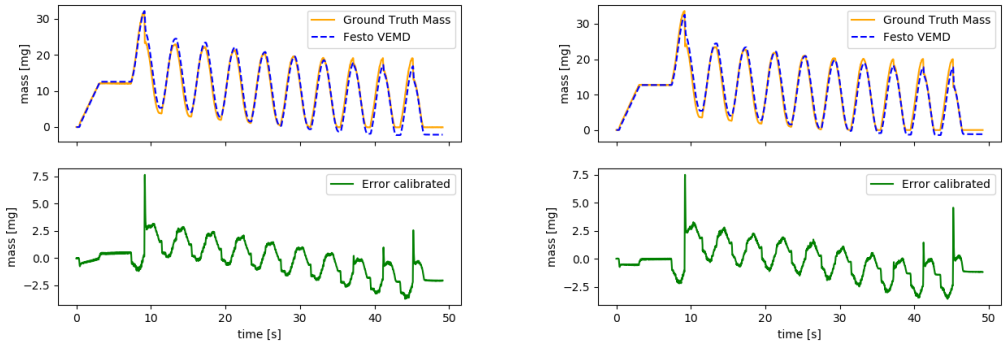

(a) Test tube with a volume of 38.8 cm^3 **(b)** Test tube with a volume of 19.8 cm^3

Figure 6.20: Robustness of calibration for different test volumes

7 Experiments Bidirectional Mass Estimator

Based on the results of the unidirectional experiments we choose the Sensirion SFM 3400 AW and the Festo VEMD sensors for our Bidirectional tests.
For these experiments we use the same test setup as in the previous experiments. Additionally, we combine the readings of the two Festo valves as the basis for the bidirectional mass estimator.
First we test both sensors by actuation three different sinus trajectories:

1) $f(x) = (sin(0.25 \cdot x \cdot \pi + 1.5 \cdot \pi) + 1.00) \cdot 6 + 12$

2) $f(x) = (sin(0.5 \cdot x \cdot \pi + 1.5 \cdot \pi) + 1.00) \cdot 6 + 12$

3) $f(x) = (sin(1.0 \cdot x \cdot \pi + 1.5 \cdot \pi) + 1.00) \cdot 6 + 12$

Afterwards we compare the results with the existing mass estimator by actuating the same trajectories with the current setup for the RBO Hand 2.

The plots in chapter 7.1 show that the actuated trajectories are not equivalent to the targeted trajectories. This is caused by spikes from the proportional valves and will be discussed in chapter 8.

7.1 Results

7.1.1 Festo VEMD

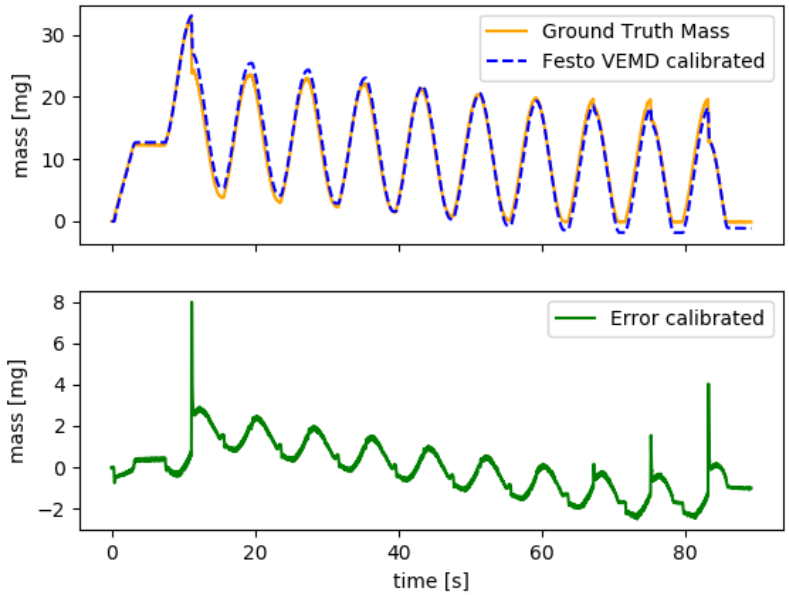

Figure 7.1: Bidirectional Mass Estimation Festo VEMD - Trajectory 1

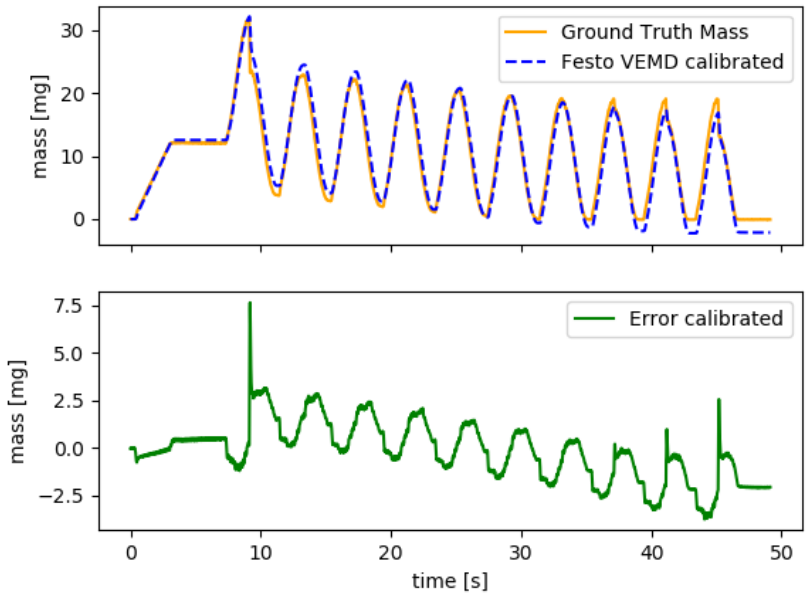

Figure 7.2: Bidirectional Mass Estimation Festo VEMD - Trajectory 2

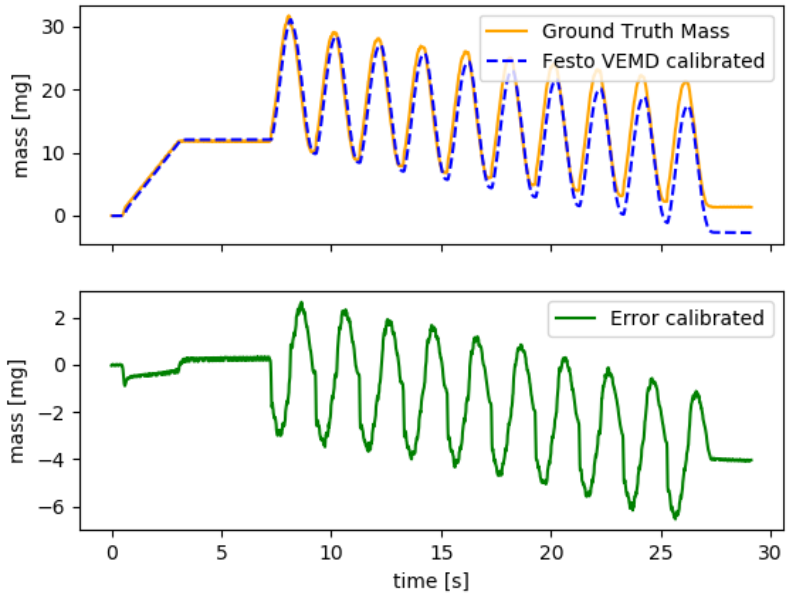

Figure 7.3: Bidirectional Mass Estimation Festo VEMD - Trajectory 3

7.1.2 Sensirion SFM 3400 AW

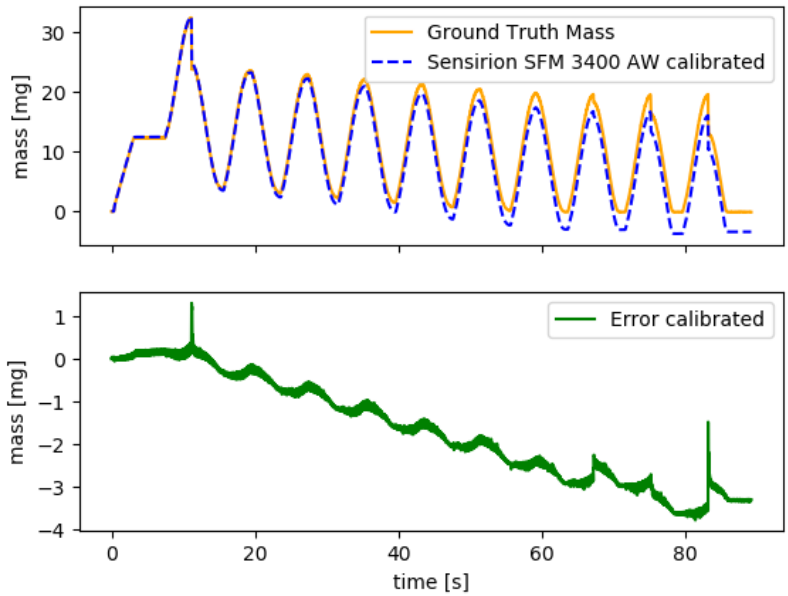

Figure 7.4: Bidirectional Mass Estimation Sensirion SFM 3400 AW - Trajectory 1

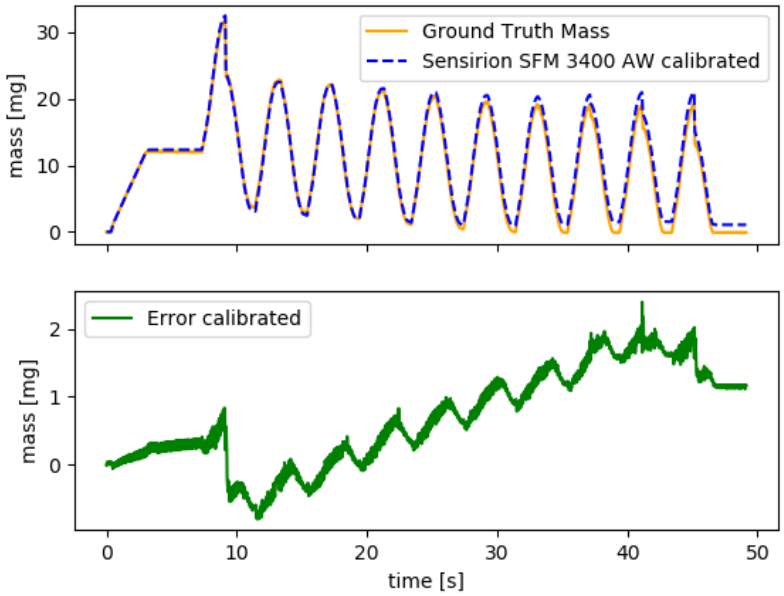

Figure 7.5: Bidirectional Mass Estimation Sensirion SFM 3400 AW - Trajectory 2

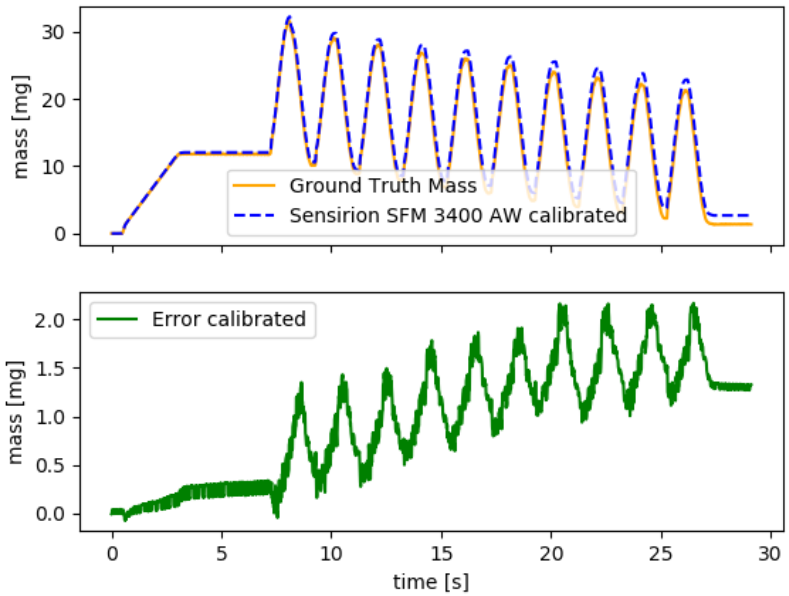

Figure 7.6: Bidirectional Mass Estimation Sensirion SFM 3400 AW - Trajectory 3

7.1.3 Discussion

To achieve a good precision with both sensors for a bidirectional mass estimation, it is necessary to calibrate both flow directions separately. For the Festo estimator this is to be expected since it consists of two sensors. Surprisingly, it is also required for the Sensirion SFM 3400 AW. This indicates that the flow profiles inside the system are different for inflation and deflation and therefore cause different errors in the sensor readings. For the Sensirion SFM 3400 AW, this error is amplified by the fact that the sensor has different diameters for both pneumatic connectors.
With the secondary calibration, the precision is similar to the unidirectional. Again, both estimators become less precise for trajectory 3 as it actuates the highest air mass flows.

7.2 Comparison with the Data-Driven Mass Estimator

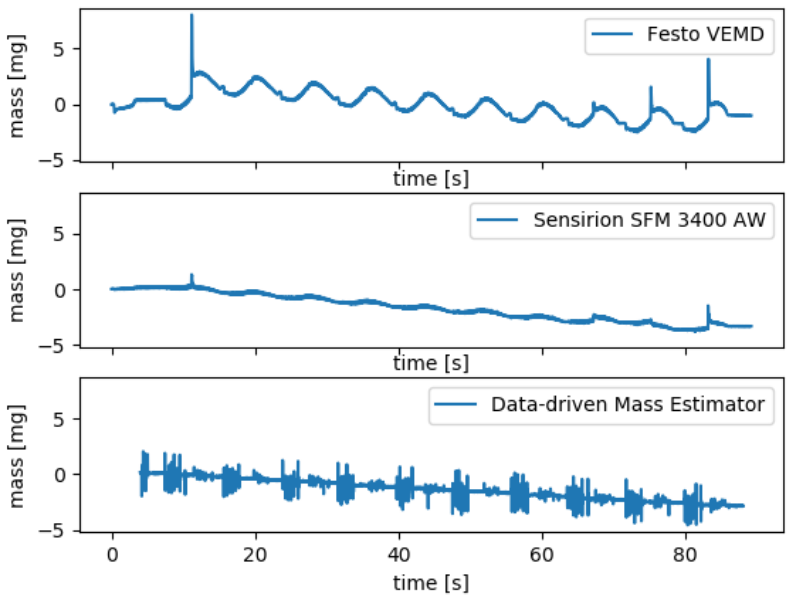

Figure 7.7: Comparison Mass Estimation - Trajectory 1

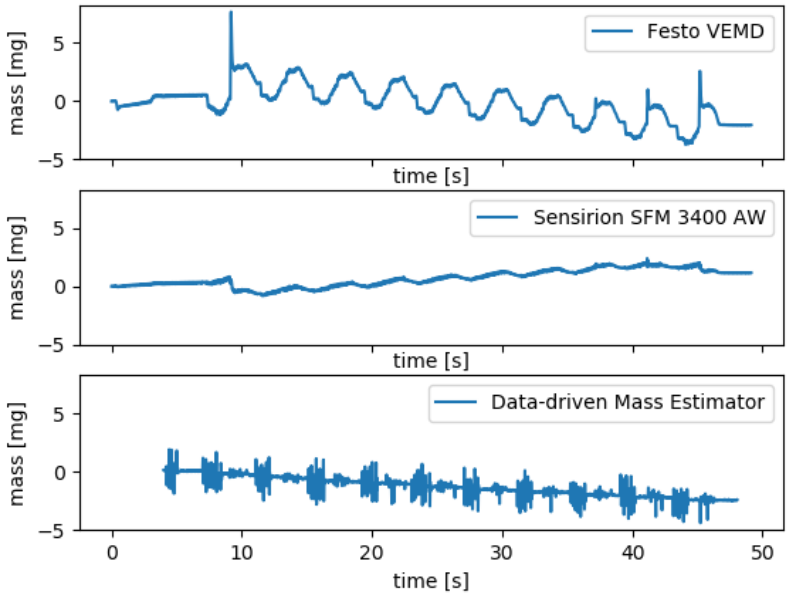

Figure 7.8: Comparison Mass Estimation - Trajectory 2

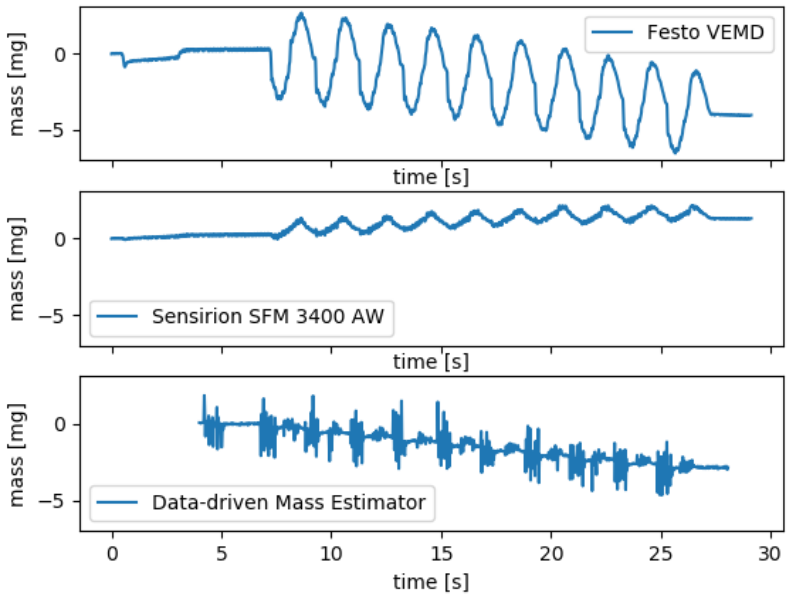

Figure 7.9: Comparison Mass Estimation - Trajectory 3

For trajectories 1 and 2, the mass estimator based on the Festo VEMD has the highest precision while having a comparable performance to the data-driven estimation of trajectory 3.

The Sensirion SFM 3400 AW has the worst precision for trajectory 1. For trajectory 2 it is slightly better than the data-driven estimator. It has the best result for trajectory 3 out of the three estimators. This indicates that the calibration has a "sweet spot" for higher mass flows.

8 Evaluation Proportional Valves

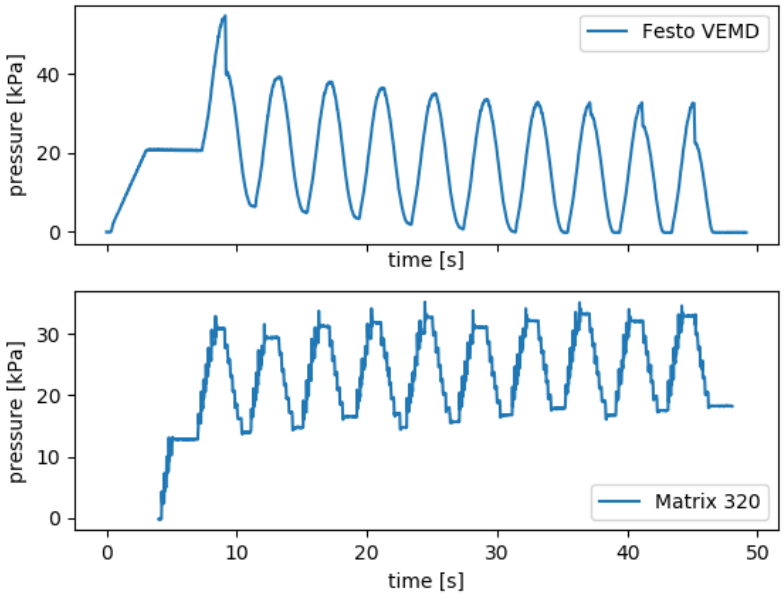

Figure 8.1: Pressure profile of different valves

Figure 8.1 shows the pressure graphs for the proportional Festo VEMD valves and binary Matrix 320 valves currently used to actuate the RBO Hand 2. The upper graph is mostly smooth while the lower has a lot of small spikes. This stems from the need to open the binary valves in a rapid fashion to achieve a median flow lower than the maximum. This translates to a noticeable shiver in the motion of a finger which is a disadvantage if a precise motion or actuation of an object is desired. This behaviour is non-existent if the Festo VEMD valve is used.

During our tests, the Festo valves tended to spike for the first actuation after a restart of our experiment setup. Smaller spikes also appeared after opening the valve from a fully closed state, especially for deflation. As the control mechanism is bundled with the included sensor, we were not able to fix this problem. According to the manufacturer, this is caused by the control flow as the valves are designed for medical use and the actuation of a constant flow rather than a rapidly changing trajectory.

9 Conclusion

We tested different air mass flow sensors and a proportional valve for their use in controlling the RBO Hand 2. Our experiments show that out of the box only one sensor is able to measure the air mass flow with an adequate precision. Tests point towards errors caused by disadvantageous flow profiles in our pneumatic circuit. More robust seem sensors with pneumatic connectors that do not require adapters with a large diameter change like the Sensors inside the Festo VEMD valves. Sensors with a custom flow path like the Omron D6F-P0010A1 also tend to be less influenced by these conditions. A more in-depth analysis of the fluid mechanical properties might help to better understand and reduce the impact of this error. Nevertheless, with a simple calibration we are able to measure air mass flow and estimate air mass in a pneumatic system with sufficient precision for the task of controlling a soft pneumatic finger. The mass estimator based on either Festo VEMD or the Sensirion SFM 3400 AW has a at least similar performance to the existing data-driven estimator.
The actuation using proportional valves shows a significant improvement in smoothness of the motion compared to the currently used binary valves and should be considered as a replacement. The Festo VEMD proportional flow control valves are not suitable for the actuation of a fast changing trajectory. Other proportional valves that can be directly controlled are available and might be taken into consideration [22][23]. Also, a combination of the data-driven estimator and proportional valves has the potential to improve the mass control without the need of additional sensors.
Considering the results of our experiments, we suggest a solution consisting of a proportional valve, a separate airflow sensor and a custom control flow to improve the mass control of the RBO Hand 2.

Bibliography

[1] Gursel Alici. Softer is harder: What differentiates soft robotics from hard robotics? *MRS Advances*, 3(28):1557–1568, Jun 2018.

[2] Helmut Hauser and Francesco Corucci. Morphosis—taking morphological computation to the next level. pages 117–122. Springer International Publishing, September 2016.

[3] Keyan Ghazi-Zahedi, Raphael Deimel, Guido Montúfar, Vincent Wall, and Oliver Brock. Morphological computation: The good, the bad, and the ugly. In *2017 IEEE/RSJ International Conference on Intelligent Robots and Systems (IROS)*, pages 464–469, 2017.

[4] Raphael Deimel and Oliver Brock. A novel type of compliant and underactuated robotic hand for dexterous grasping. *The International Journal of Robotics Research*, 35(1-3):161–185, 2016.

[5] Raphael Deimel, Marcel Radke, and Oliver Brock. Mass control of pneumatic soft continuum actuators with commodity components. In *2016 IEEE/RSJ International Conference on Intelligent Robots and Systems (IROS)*, pages 774–779. IEEE, 2016.

[6] Raphael Deimel. *Soft robotic hands for compliant grasping.* Doctoral thesis, Technische Universität Berlin, Berlin, 2017.

[7] Thomas George Thuruthel, Yasmin Ansari, Egidio Falotico, and Cecilia Laschi. Control strategies for soft robotic manipulators: A survey. *Soft Robotics*, 5(2): 149–163, 2018.

[8] Daniela Rus and Michael T. Tolley. Design, fabrication and control of soft robots. *Nature*, 521(7553):467–475, May 2015.

[9] Morgan T. Gillespie, Charles M. Best, Eric C. Townsend, David Wingate, and Marc D. Killpack. Learning nonlinear dynamic models of soft robots for model predictive control with neural networks. In *2018 IEEE International Conference on Soft Robotics (RoboSoft)*, pages 39–45, 2018.

[10] Dongshuo Li, Vaishnavi Dornadula, Kengyu Lin, and Michael Wehner. Position control for soft actuators, next steps toward inherently safe interaction. *Electronics*, 10(9), 2021. doi: 10.3390/electronics10091116.

[11] N.T Nguyen. Micromachined flow sensors—a review. *Flow Measurement and Instrumentation*, 8(1):7–16, 1997.

[12] Y.U. Lim, Y.J. Cho, and S.H. Lee. Design and fabrication of a drag force type air flowmeter with polyoly -silicon piezoresistive iezoresistive iezoresistive layer. *International Journal of Mechanical and Mechatronics Engineering*, 18:89–94, 01 2018.

[13] P. Enoksson, G. Stemme, and E. Stemme. A silicon resonant sensor structure for coriolis mass-flow measurements. *Journal of Microelectromechanical Systems*, 6(2):119–125, 1997.

[14] B.W. van Oudheusden. Silicon thermal flow sensors. *Sensors and Actuators A: Physical*, 30(1):5–26, 1992.

Internet

[15] https://www.mouser.de/datasheet/2/307/en_d6f_series-1128136.pdf (Last accessed: 2021-11-16)

[16] https://sensing.honeywell.com/mass-flow-vs-volumetric-flow-and-unit-conversion-tn-008043-2-en-final-06nov12.pdf (Last accessed: 2021-11-16)

[17] https://www.festo.com/cat/en-gb_gb/data/doc_ENGB/PDF/EN/VEMD-G_EN.PDF (Last accessed: 2021-11-16)

[18] https://sensing.honeywell.com/honeywell-sensing-airflow-awm50000-series-catalog-pages.pdf (Last accessed: 2021-11-16)

[19] https://posifatech.com/wp-content/uploads/2020/11/210401_Datasheet_PMF83000_MassAirFlowSensor_Rev1_C3.pdf (Last accessed: 2021-11-16)

[20] https://www.sensirion.com/fileadmin/user_upload/customers/sensirion/Dokumente/5_Mass_Flow_Meters/Datasheets/Sensirion_Mass_Flow_Meters_SFM3400_Datasheet.pdf (Last accessed: 2021-11-16)

[21] https://www.sensirion.com/fileadmin/user_upload/customers/sensirion/Dokumente/5_Mass_Flow_Meters/Application_Notes/Sensirion_GF_AN_SFM-01_Engineering_Guidelines_For_Mass_Flow_Meters_D1.pdf (Last accessed: 2021-11-16)

[22] https://www.staiger.de/media/com_staiger_products-files/VP%20204-506_de.pdf (Last accessed: 2021-11-16)

[23] https://kellypneumatics.com/download_files/MPVspec.pdf (Last accessed: 2021-11-16)